Hindawi
Advances in Materials Science and Engineering
Volume 2018, Article ID 6950876, 9 pages
https://doi.org/10.1155/2018/6950876

Research Article

Influence of Carbon Addition to Fe-Mn-Si Type Alloy on the Structure and Shape Memory Effect

Witold Prendota,[1,2] **Kamil Goc**,[1,2] **Shunsuke Miyazawa**,[2] **Akito Takasaki**,[2] **Damian Rybicki**,[1] **and Czeslaw Kapusta**[1]

[1]*AGH University of Science and Technology, Faculty of Physics and Applied Computer Science, Department of Solid State Physics, Al. Mickiewicza 30, 30-059 Krakow, Poland*
[2]*Shibaura Institute of Technology, Department of Engineering Science and Mechanics, 3-7-5 Toyosu, Koto-ku, Tokyo 135-8548, Japan*

Correspondence should be addressed to Witold Prendota; witold.prendota@fis.agh.edu.pl

Received 18 July 2018; Accepted 12 September 2018; Published 10 October 2018

Academic Editor: Ivan Gutierrez-Urrutia

The study presented is focused on the influence of carbon addition on properties of the Fe-Mn-Si type intelligent materials with basic composition of Fe64Mn30Si6 (wt. %). Three alloys were prepared, starting from elemental powders, with 0, 0.1, and 0.3 wt. % of carbon, at corresponding silicon content reduction. For the synthesis, the mechanical alloying, sintering, and annealing were applied. Further process involved deformation and subsequent heating in a furnace. High temperature X-ray diffraction patterns, obtained at room temperature and up to 600°C, showed evolution of α', γ, and ε phase peaks. The study revealed that a small carbon addition (of 0.1 wt. %), could increase shape recovery stress, even up to 1.8% after one cycle of training. The higher carbon content leads to a deterioration of the property. Also, relative density differences are observed between the sintered Fe64Mn30Si6 (wt. %) alloys with before/after annealing with/without mechanical alloying involvement.

1. Introduction

The family of alloys exhibiting shape memory effect (SME) has a wide range of industrial applications, such as the medical, the energy fields, etc. [1–7]. The SME of the Fe-Mn-Si alloy system has been discovered by Sato et al. in 1982 [8–10]. Because the alloying elements (Fe, Mn, and Si) are relatively inexpensive, this system has been expected to be a promising alternative to expensive Ti-Ni-based shape memory alloys. In addition to the low cost, this system has excellent properties in its machinability, formability, weldability, corrosion resistance, and high strength. The Fe-Mn-Si based alloys possess one way SME that is why they are used as various structural materials such as main fastening material pipe fittings or seismic alloy [11].

While the SME of the Ti-Ni-based alloys occurs due to a thermoelastic martensitic phase transformation, that in the Fe-Mn-Si alloys originates from a stress-induced γ (fcc) $\longrightarrow$ ε (hcp) martensitic transformation, followed by an $\varepsilon \longrightarrow \gamma$ reverse transformation during heating. Stress-induced martensitic transformation occurs by the creation of stacking faults (SFs) due to the movement of the Shockley partial dislocations (a/6 <112>FCC) in the parent phase. Stress-induced martensitic transformation in the Fe-Mn-Si shape memory alloys was found to occur at the deformation within 3-4% [10, 12, 13], and the optimization of composition for the maximum shape memory effect has been made. Basic composition in this type of alloy system has been established at the Fe(61–66)Mn(28–33)Si6 (wt. %) [10, 14]. Moreover, the improvements have been reported for this alloy system by the addition of rare earth elements (RE) [15] and other methods [16–18]. However, the usage of expensive RE elements, even with expected improvement in shape memory characteristics, makes that the attractiveness of the Fe-Mn-Si alloys related to their low cost is lost.

Fe-Mn-Si shape memory alloys have been used in various fields, as described above. Most of them are manufactured using a wire or plate made by the dissolution

method [8–10, 14, 19–24]. In the conventional melting method, it poses a problem with their manufacturing as will be discussed. First, because Fe is very reactive, the selection of dissolution atmosphere and crucible is critical. In addition, the appearance of composition variation and impurities in the ingot is likely. Moreover, because the manufacturing process is large-scaled, it is difficult to shape the material properly. Therefore, production using powder metallurgy methods as a solution to the abovementioned problems has been attempted. This method has shown to possess various advantages in the manufacturing of industrial products. Its main feature is the possibility to obtain a uniform composition of materials, which can be manufactured with near net shape. Owing to this, it is considered as one of the methods that can solve the abovementioned problems. It also minimizes the additional usage of machining usually required to form the final product, in comparison with casting techniques. Therefore, it is worth exploring as the alternative production route for the Fe-Mn-Si shape memory alloys. The mechanical alloying (MA) technique is easy in processing and making some composition adjustment to the alloy. During MA, the high energy collisions between ball and elemental particles occur. Consequently, with the repeated cold welding and fracture of the powder grains, not only the alloying process is attained, but also the synthesis of the nonequilibrium structures (such as supersaturated solid solutions, intermetallic compounds, nanocrystalline, and amorphous structures) is possible [25, 26]. This offers many advantages, such as reduced grain size, the formation of intermetallic compounds, the ability to synthesize alloys from elements with much different melting points, and the capability of producing nano-sized structures [27]. These characteristic advantages can lead to excellent mechanical features as well as other unique properties of the products.

The rotational speed required for a Fe-Mn-Si powder production by MA method and manufacturing conditions (e.g., the milling time) has been reported by Saito et al. [25, 27] To produce Fe-Mn-Si shape memory alloys in this study, mechanical alloying and pulse electric current sintering methods have been used. Instead of using expensive elements such as abovementioned rare earths, addition of inexpensive carbon to Fe-Mn-Si system was investigated in this work, expecting an improvement of its properties by strengthening the matrix phase with a solid solution. In addition, usage of thermomechanical processing was investigated for the purpose of shape memory properties improvement.

2. Materials and Methods

In this study, commercially available electrolytic Fe (99.9%), electrolytic Mn (99.9%), atomized Si (99.9%), and scaly graphite carbon (99.9%) elemental powders were used. Three kinds of samples of compositions listed in Table 1, were prepared by MA.

The powder was milled using a planetary ball mill (Pulverisette 7, Fritsch) with a stainless steel vial (volume = 45 ml). The ball-to-powder weight ratio was 8 : 1. The powder mixture was milled with stainless steel balls (15 mm diameter) in the atmosphere of Ar gas at a rotational speed of 600 rpm. The mechanically alloyed powder obtained (MA powder) was put into a graphite die and sintered by means of pulse-current pressure sintering equipment (PLASMAN, SS Alloy). The sintering was performed for a period of time of 600 s at the temperature of 1173 K in vacuum conditions (2 Pa) under an external uniaxial compression pressure of 20 MPa. The sample obtained was cylindrical with a diameter of 10 mm and a height of about 20 mm. Since the sintered bulk alloy was subjected to stress during sintering, the alloy was then annealed in a furnace at 873 K for 3600 s under high vacuum conditions (10^{-3} Pa) to relieve the resulting internal stress.

Table 1: Chemical compositions of the alloys.

Alloy	Elements (wt. %)			
	Fe	Mn	Si	C
1	64	30	6	—
2			5.9	0.1
3			5.7	0.3

The crystallographic phase analysis was carried out with X-ray diffraction (XRD) equipment (Ultima IV, Rigaku), at room temperature, using Cu-Kα radiation (wavelength λ = 0.154 nm) at 40 kV and 45 mA with a graphite monochromator.

X-ray fluorescence (XRF) analysis was performed on SEA1000A (SII Nanotechnology Inc.) apparatus. It allowed us to determine the elemental composition (except for carbon) of the samples. Scanning electron microscopy (SEM, JSM-7001F, JEOL) with energy-dispersive X-ray spectroscopy (EDS, JED-2300, JEOL) for determination of distribution of individual elements and surface morphology analysis of powders and bulk samples was also performed.

The SME of the bulk alloy was characterized by shape recovery strain after 4% deformation and subsequent heating in a furnace at 923 K. The deformation was achieved at room temperature by compression in the uniaxial geometry, parallel to the external stress exerted at the sintering. The shape recovery strain was determined from the change in the height during heating divided by the initial height before deformation. The following expression was used for its calculation:

$$\text{shape recovery strain}\,[\%] = \frac{h_2 - h_1}{h_0} \times 100, \tag{1}$$

where h_0 is the initial height before deformation, h_1 is the height after deformation, and h_2 is the height after the subsequent heating. The h_0, h_1, and h_2 were measured with a screw micrometer at five points for each height to evaluate the standard error at room temperature.

3. Results and Discussion

3.1. Analysis of Elemental Composition. XRF measurement results of the MA powder and bulk alloy without addition of C are shown in Table 2. The compositions of both the Fe-Mn-Si powder and bulk alloy were almost close to as

Table 2: XRF analysis results of MA processed powder and sintered alloy.

Form	Elements (wt. %)					
	Fe		Mn		Si	
	Con	AE	Con	AE	Con	AE
Powder	64.43	0.43	29.94	0.06	5.63	0.37
Bulk	63.22	0.78	30.33	0.33	6.45	0.45

Con, concentration; AE, absolute error.

weighted content Fe : Mn : Si = 64 : 30 : 6 (wt. %), showing that substantially uniform composition of the alloy is obtained. The results of elemental analysis of MA processed powders are shown in Figure 1. For each powder, all the elements are evenly distributed, which suggests that it is uniformly mixed. The determined composition of the powder and bulk samples is consistent with that obtained by XRF.

3.2. Characteristics of the Alloy Sintered Directly from Elemental Powders. In this section, we describe the properties of the alloy obtained by using pulse electric current sintering elemental powders of Fe-Mn-Si system, without preceding MA treatment. The results of EDX analysis are shown in Figure 2. They reveal uneven distribution of iron, visible as dark paths. These features correspond to increased silicon content (red and pink color), whereas manganese appears to be more evenly distributed. The sample has subsequently been subjected to chemical polishing in a solution. Results of the EDX analysis of the sample treated in such a way are shown in Figure 3. Chemical polishing does not remove the iron deficient regions that are still well visible, whereas it generally decreases the silicon surficial content. No visible influence of this chemical polishing procedure on the manganese content is noted.

3.3. Impact of the MA of the Powder on the Sintered Alloy Characteristics. As obtaining metallographically homogeneous sintered sample directly from mixture of elemental powders appeared to be unsuccessful, we have tried to process the powder mixture with MA using a planetary ball mill. The results of a metallographic study of the alloy sintered from such a powder and the alloy sintered and subsequently annealed are shown in Figures 4 and 5. The EDX maps reveal that the distribution of constituent elements in the material is homogeneous. In particular, no regions deficient in iron are observed, in contrast to the alloy sintered from the MA untreated powders. Thus, by MA, it is possible to achieve a significant improvement of the microstructural homogeneity of the alloy.

3.4. Estimation of Alloys Density. The results of measurements of the sintered alloys density, which were obtained with the Archimedes' method are shown in Figure 6. The relative density of the sintered alloy (without MA treatment of the starting powder) before annealing is about 98% (Figure 6(a)) and about 95% after its annealing (Figure 6(b)). Densities of alloys obtained from MA treated powders are shown in Figures 6(c) and 6(d) and reach 98 and 99% for the sintered alloy before annealing and after annealing, respectively. Difference in densities for sintered alloys, before annealing and after annealing (without MA treating of the starting powders), can be attributed to gaps made by Kirkendall effect during solution treatment. It is worth noting that the alloy sintered from the MA treated powders shows a relative density of almost 100% after annealing. Thus, by MA, it is possible to achieve a significant improvement of the density of these shape memory alloys.

3.5. Improvement of Shape Recovery Characteristics with C Addition. It is well known that characteristics of the shape memory alloy can vary significantly, depending on their composition. In Fe-Mn-Si system, alteration of the properties by the addition of elements is possible. In particular, the parent phase reinforcement with a solid solution with C addition is known to improve the shape memory characteristic [28].

Magnetic properties of the MA powders and the sintered alloys produced were investigated with Mössbauer spectroscopy. Mössbauer spectra for MA10h and MA30h of Fe-30Mn-5.9Si-0.1C (wt. %) are shown in Figures 7 and 8, respectively. The spectrum after 10 h of MA shows a weak sextet and a dominant single peak which correspond to the ferromagnetic and the paramagnetic (or diamagnetic) component, respectively. This reveals presence of a mixture of α and γ phases, showing that MA process was incomplete. For the Mössbauer spectrum of the powder subjected to MA for 30 h, only a single paramagnetic peak is observed, and the ferromagnetic component seen for the powder after 10 h of MA did not appear. Therefore, it can be concluded that the formation of the γ phase is complete for the 30 h of MA.

Annealed alloy samples with 0 and 0.1% carbon content have also been investigated by Mössbauer spectroscopy. Results obtained from room temperature (RT) and 80 K measurements are shown in Figure 9. A single peak is observed for all the spectra. Differences of isomer shift (listed in Table 3) observed at both temperatures indicate, that carbon enters the bulk of the alloy. This is also consistent with a larger line width observed for the carbon containing sample. For both samples, a significant broadening of the spectrum (by more than two times) on lowering the temperature from 293 K to 80 K is observed, which can be attributed to a slowing down of the paramagnetic fluctuations.

The crystallographic structure of the bulk alloy synthesized from the MA treated powder and subjected to the compressive strain was studied with high-temperature X-ray diffraction. The XRD patterns for Fe-30Mn-5.9Si-0.1C (wt. %) alloy at several heating temperatures are shown in Figure 10. Figure 10(a) shows an XRD pattern of the bulk alloy after 4% deformation. All the peaks are broad and the ε phase peaks are pronounced. Peaks broadening indicates an increase in lattice strain due to decreasing temperature. Furthermore, since the ε phase peaks are relatively large, it

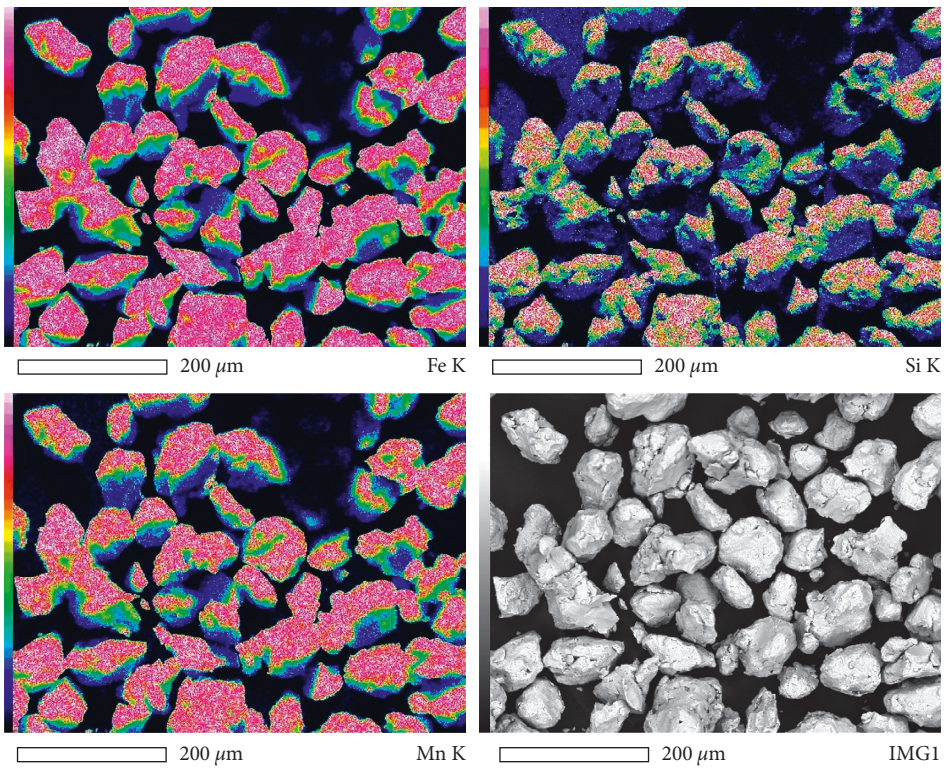

Figure 1: SEM and EDX analysis of Fe-30Mn-6Si MA powders.

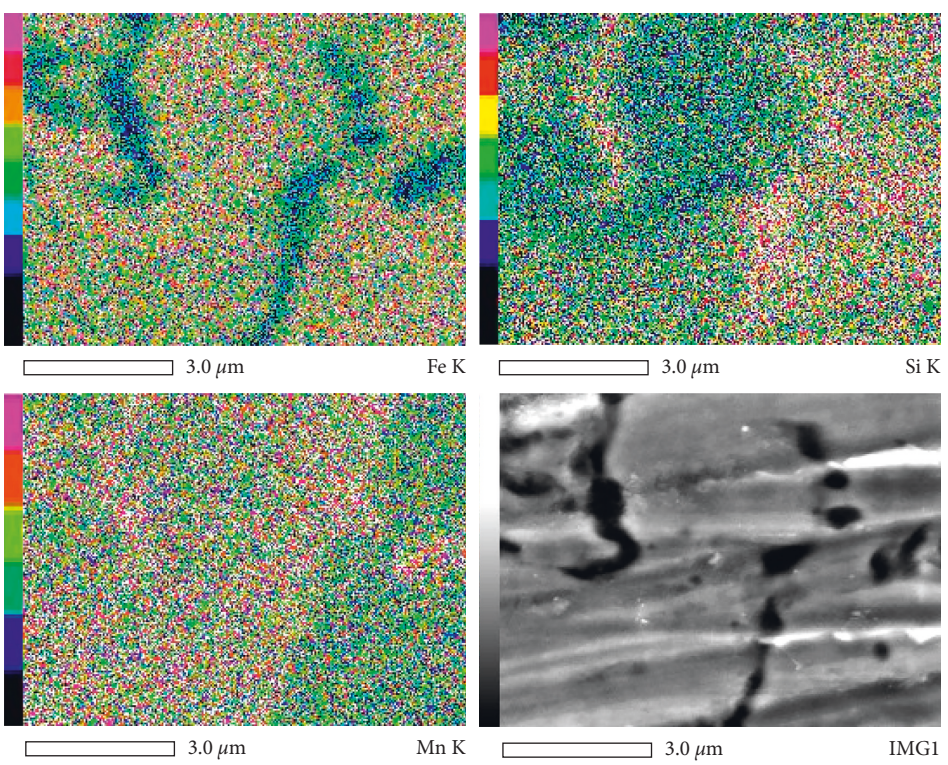

Figure 2: SEM and EDX analysis of Fe-30Mn-6Si bulk alloy after sintering without preceding MA treatment.

suggests that $\gamma \longrightarrow \varepsilon$ stress-induced martensitic transformation due to the deformation occurred. With increasing heating temperature, the intensities of ε phase peaks are decreasing and, eventually, the ε phase peaks disappear when the sample is heated at 600°C. In contrast to that, the diffraction peaks of the γ phase continue to increase with

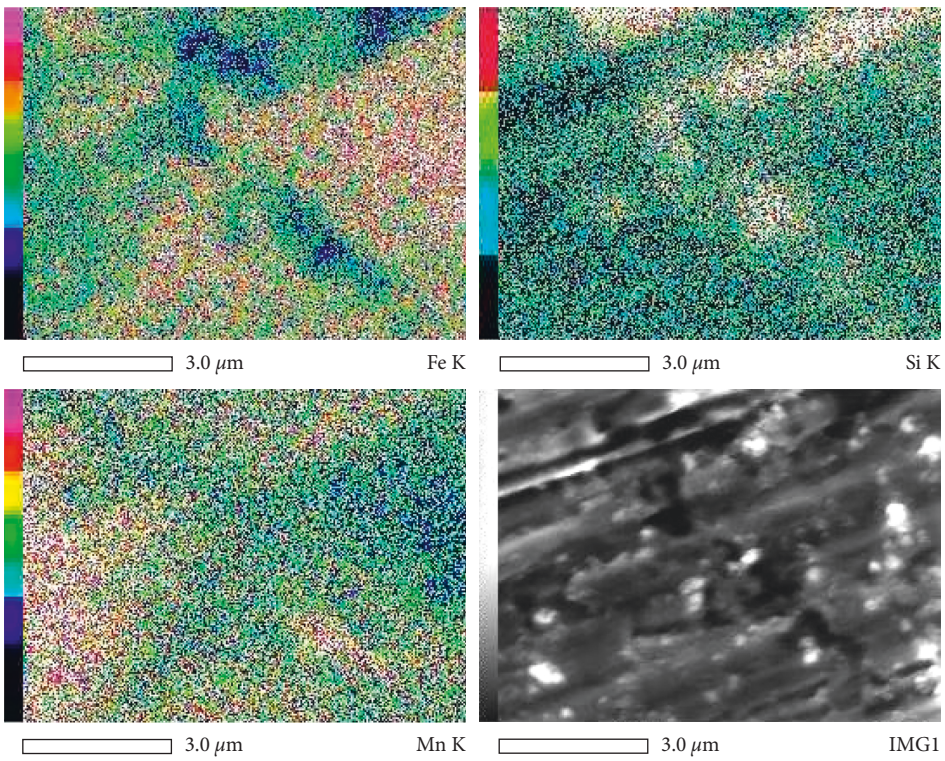

Figure 3: SEM and EDX analysis of Fe-30Mn-6Si bulk alloy after sintering and annealing with preceding MA treatment.

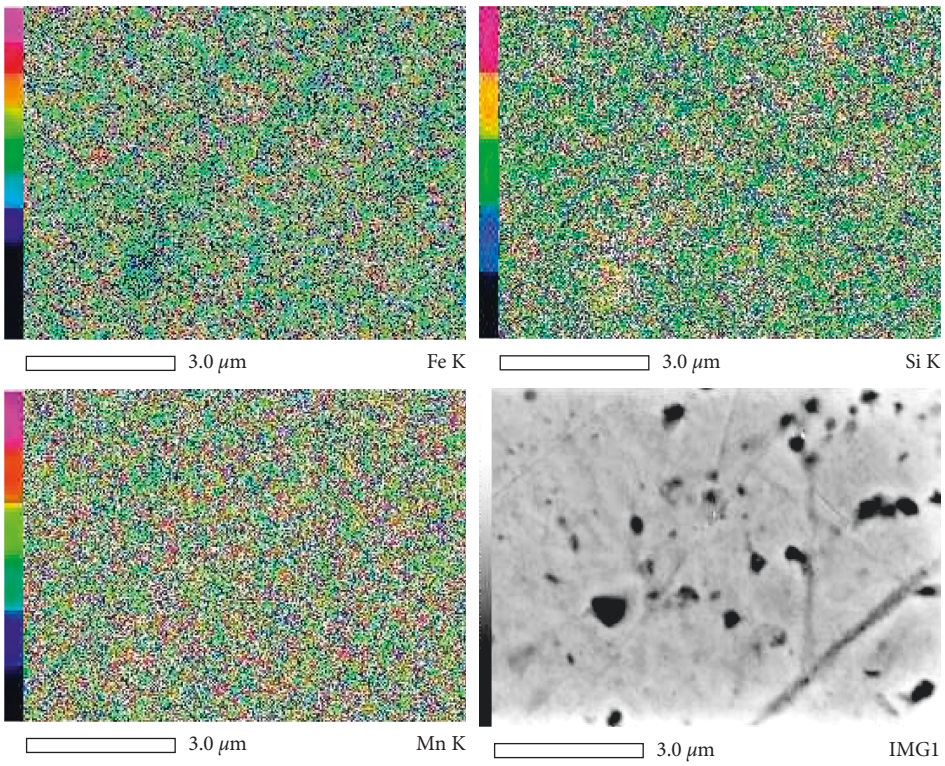

Figure 4: SEM and EDX analysis of Fe-30Mn-6Si bulk alloy after MA and subsequent sintering.

increasing temperatures and a sharp peak is observed at temperatures higher than 400°C. Thus, with the heating, the amount of ε phase is reduced, but the γ phase increases its content, suggesting that the $\varepsilon \longrightarrow \gamma$ reverse transformation occurred. So, these high temperature X-ray diffraction results indicate that this alloy may have a shape memory.

However, for using it as an industrial product, shape recovery strain is an important factor. The shape recovery

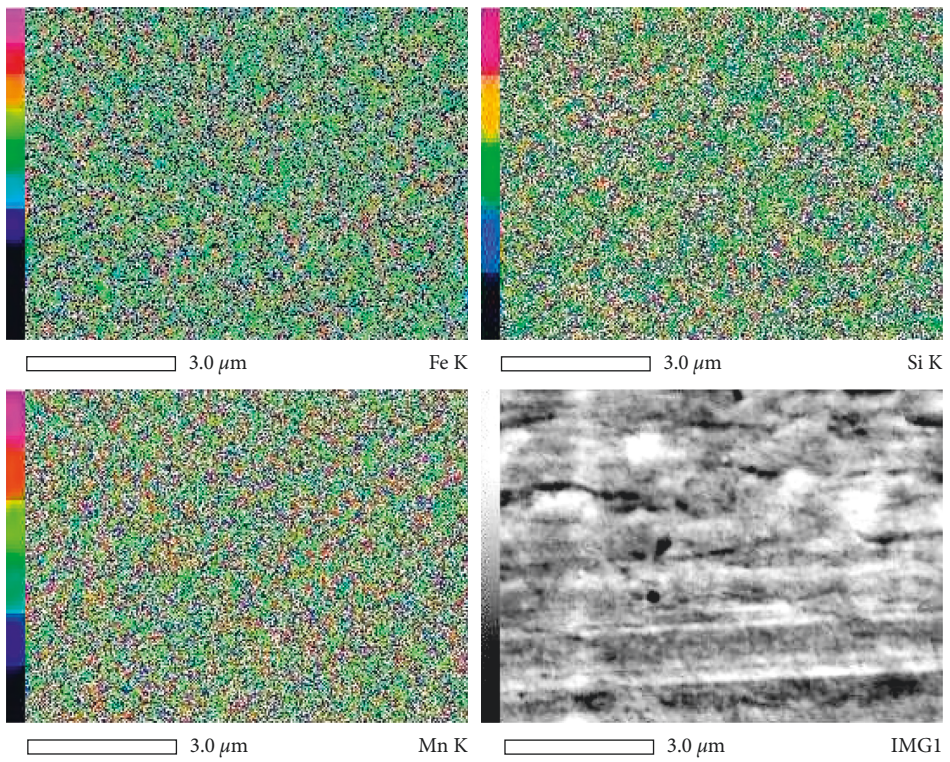

Figure 5: SEM and EDX analysis of Fe-30Mn-6Si bulk alloy after MA, sintering, and annealing.

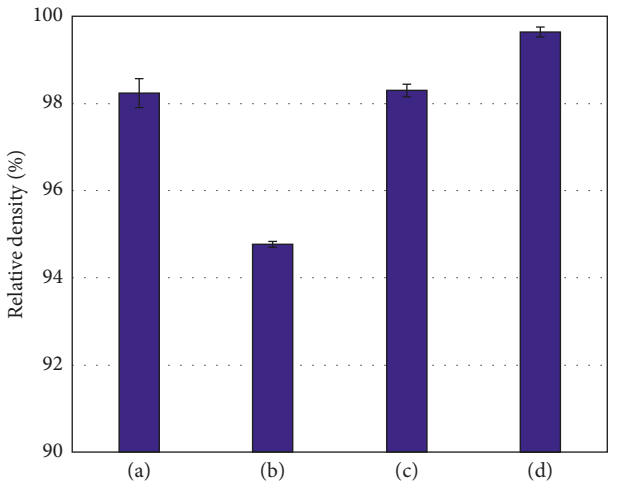

Figure 6: Change in relative density (with standard deviation) of sintered alloys (a) before annealing without preceding MA treatment, (b) after annealing without preceding MA treatment, (c) before annealing with MA treatment, and (d) after annealing with MA treatment.

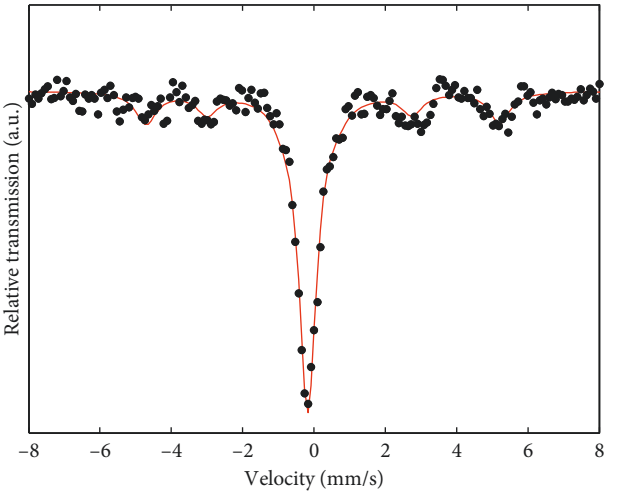

Figure 7: Mössbauer spectra for Fe-30Mn-5.9Si-0.1C powders after MA for 10 h.

strain characteristics for the bulk alloy with C addition is shown in Figure 11(a). It increased with increasing carbon concentration up to 0.1 wt. %. The maximum shape recovery strain obtained is about 1.5%. This result exceeds those of the basic composition we have previously reported [27]. Figure 11(b) presents the curve of shape recovery strain after one cycle of training, which is similar to previously mentioned curve for the annealed state. The improvement of this parameter up to about 1.8% for the alloy with 0.1 wt. % of carbon is shown.

3.6. Improvement of Shape Recovery Characteristics with Thermomechanical Processing. As described above, it was possible to obtain an improvement of the shape recovery characteristics by C addition. However, for the industrial use, shape recovery strain of more than 2% is required [29]. Therefore, for a further improvement of the shape recovery characteristics, it is necessary to attempt thermomechanical

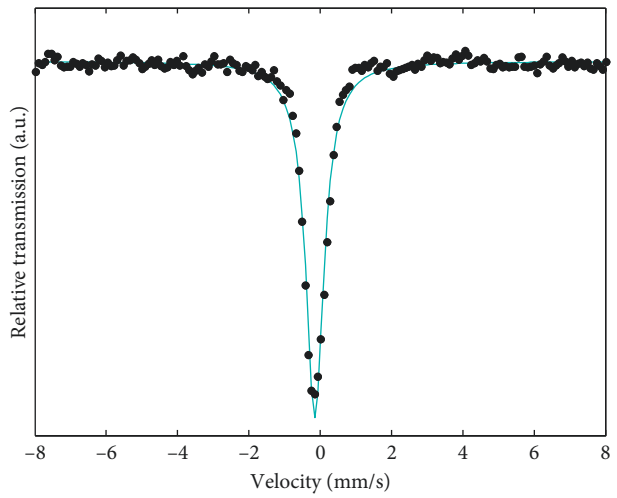

Figure 8: Mössbauer spectra for Fe-30Mn-5.9Si-0.1C powders after MA for 30 h.

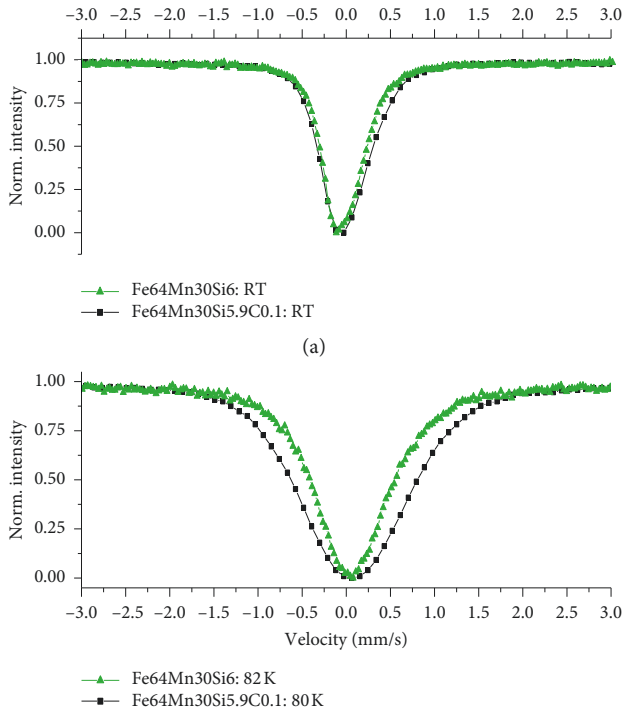

Figure 9: Mössbauer spectra: (a) room temperature and (b) 80 K for Fe-30Mn-6Si and Fe-30Mn-5.9Si-0.1C alloys after annealing.

Table 3: Isomer shift values at room temperature and 80 K.

Sample	Isomer shift value at room temperature (mm/s)	Isomer shift value in 80 K (mm/s)
Fe64Mn30Si6	0.0007 ± 0.0019	0.0472 ± 0.0024
Fe64Mn30Si5.9C0.1	−0.0253 ± 0.0091	0.1249 ± 0.0026

processing. For this purpose, the sintered alloy was subjected to annealing. Owing to this, the critical stress for slip is low and the material is susceptible to plastic deformation due to

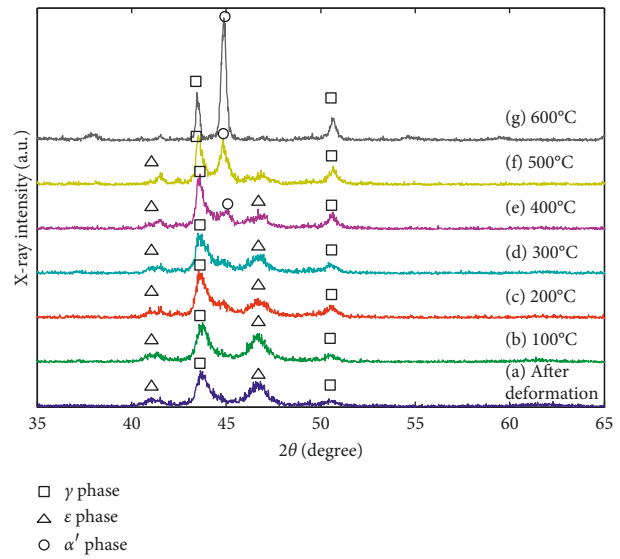

Figure 10: High temperature XRD patterns for Fe-30Mn-5.9Si-0.1C alloy at several heating temperatures.

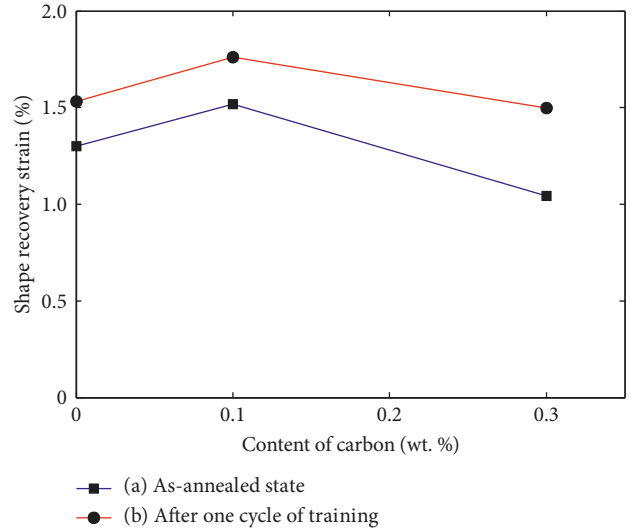

Figure 11: Dependence of shape recovery strain on C content of the alloys. (A) As-annealed state. (B) After one cycle of training.

slip. In this situation, we deal with low state of critical stress, and it is difficult to impart suitable shape memory properties. The material was further subjected to thermomechanical processing for increase of the critical stress for slip. Shape recovery strain characteristics after the thermomechanical process, as shown in Figure 11(b), can be greatly improved. In particular, the alloy with the addition of 0.1 wt. % C significantly improved its properties. Shape recovery strain of this sample (Fe-30Mn-5.9Si-0.1C), which was subjected to thermomechanical process, is of 1.8%. Although this is still less than the strain required to a structural material, it was confirmed that the shape recovery performance was improved. So that, with the C addition and training process, a potential was shown for future application of the fabricated shape memory alloy.

4. Summary and Conclusions

In this study, we investigated the possibility of the practical use of the Fe-Mn-Si-based shape memory alloy, which is manufactured by the MA method. Elemental analysis of the prepared powders and bulk alloys, characteristics such as density of the alloys and shape recovery strain were investigated. The following findings were obtained:

(i) By using MA powder, it was shown that it is possible to produce an alloy with high density and homogeneous metallographic nature.

(ii) In order to improve shape recovery properties, small amount of carbon was added as a fourth element and a comparison with basic composition (Fe-30Mn-6Si, wt. %) was made. The improvement is confirmed up to 0.1 wt. % of carbon. Higher concentration was resulting in a reduction of shape recovery strain value, which is in good agreement with alpha phase creation, as stems from iron-carbon phase diagram. Mössbauer spectroscopy measurements confirmed that carbon entered the bulk of the alloy.

(iii) The thermomechanical training process leads to the increase of the shape recovery strain for all the samples (up to 0.3 wt. % of carbon), when compared to samples without training. The alloy with Fe-30Mn-5.9Si-0.1C (wt. %) composition exhibits the biggest shape recovery strain, which is of 1.8%.

(iv) Different durations (10 and 30 hours) of mechanical alloying of powders with carbon addition (0.1 wt. %) reveal changes in their phase composition, which is reflected in their magnetic properties. Powder after shorter MA time exhibits coexistence of ferromagnetic and paramagnetic phases. Longer MA treatment smears out the ferromagnetic component, which is associated with alpha to gamma iron phase transformation. The behavior is similar in the case of carbon-doped materials.

Data Availability

No data were used to support this study.

Conflicts of Interest

The authors declare that they have no conflicts of interest.

Acknowledgments

This work was supported by the Ministry of Science and Higher Education (MNiSW), Poland, and Shibaura Institute of Technology, Japan. Damian Rybicki and Czeslaw Kapusta acknowledge the support of the Faculty of Physics and Applied Computer Science AGH UST statutory tasks no. 11.11.220.01/6 within subsidy of the Ministry of Science and Higher Education, Poland.

References

[1] H. Kyogoku, "New processing method of shape memory alloy by powder metallurgy," *Materia Japan*, vol. 47, no. 2, pp. 79–84, 2008.

[2] L. Petrini and F. Migliavacca, "Biomedical applications of shape memory alloys," *Journal of Metallurgy*, vol. 2011, Article ID 501483, 15 pages, 2011.

[3] J. W. Hu, M.-H. Noh, and J.-H. Ahn, "Experimental investigation on the behavior of bracing damper systems by utilizing metallic yielding and recentering material devices," *Advances in Materials Science and Engineering*, vol. 2018, Article ID 2813058, 15 pages, 2018.

[4] C. De Crescenzo, D. Karatza, D. Musmarra et al., "Ni-Ti shape memory alloy coatings for structural applications: optimization of HVOF spraying parameters," *Advances in Materials Science and Engineering*, vol. 2018, Article ID 7867302, 10 pages, 2018.

[5] Y.-J. Fang, X.-S. Jiang, D.-F. Mo et al., "Microstructure and mechanical properties of electron beam-welded joints of titanium TC4 (Ti-6Al-4V) and Kovar (Fe-29Ni-17Co) alloys with Cu/Nb multi-interlayer," *Advances in Materials Science and Engineering*, vol. 2018, Article ID 2042871, 11 pages, 2018.

[6] Y. J. O. Moraes, A. A. Silva, M. C. Rodrigues, A. G. B de Lima, R. P. B. dos Reis, and P. C. S. da Silva, "Dynamical analysis applied to passive control of vibrations in a structural model incorporating SMA-SE coil springs," *Advances in Materials Science and Engineering*, vol. 2018, Article ID 2025839, 15 pages, 2018.

[7] C. Zhao, F. Zhang, J. Xiong, Z. Jiang, X. Yang, and H. Cui, "Plasticity improvement of ball-spun magnesium alloy tube based on stress triaxiality," *Advances in Materials Science and Engineering*, vol. 2018, Article ID 1735046, 12 pages, 2018.

[8] A. Sato, E. Chishima, K. Soma, and T. Mori, "Shape memory effect in $\gamma \rightleftarrows \epsilon$ transformation in Fe-30Mn-1Si alloy single crystals," *Acta Metallurgica*, vol. 30, no. 6, pp. 1177–1183, 1982.

[9] A. Sato, E. Chishima, Y. Yamaji, and T. Mori, "Orientation and composition dependencies of shape memory effect IN Fe-Mn-Si alloys," *Acta Metallurgica*, vol. 32, no. 4, pp. 539–547, 1984.

[10] A. Sato, Y. Yamaji, and T. Mori, "Physical properties controlling shape memory effect in Fe-Mn-Si alloys," *Acta Metallurgica*, vol. 34, no. 2, pp. 287–294, 1986.

[11] A. Sato, H. Kubo, and T. Maruyama, "Mechanical properties of Fe-Mn-Si based SA and the application," *Materials Transactions*, vol. 47, no. 3, pp. 571–579, 2006.

[12] M. Mocanu, E. Mihalache, R.-C. Comăneci, B. Pricop, B. Özkal, and L. G. Bujoreanu, "Tensile stress-induced structural changes associated with martensite transformations in Fe-Mn-Si based shape memory alloys," *Materials Science Forum*, vol. 907, pp. 25–30, 2017.

[13] C. Leinenbach, A. Arabi-Hashemi, W. J. Lee et al., "Characterization of the deformation and phase transformation behavior of VC-free and VC-containing FeMnSi-based shape memory alloys by in situ neutron diffraction," *Materials Science and Engineering A*, vol. 703, pp. 314–323, 2017.

[14] M. Murakami, H. Otsuka, H. G. Suzuki, and M. Matsuda, "Complete shape memory effect in polycrystalline Fe–Mn–Si alloys," in *Proceedings of the International Conference on Martensitic Transformations (ICOMAT-86) (ICO-MAT-86)*, pp. 985–990, Nara, Japan, August 1986.

[15] X. Huang, Y. Lei, B. Huang, S. Chen, and T. Y. Hsu, "Effect of rare-earth addition on the shape memory behavior of a FeMnSiCr alloy," *Materials Letters*, vol. 57, no. 19, pp. 2787–2791, 2003.

[16] Y. H. Wen, H. B. Peng, D. Raabe, I. Gutierrez-Urrutia, J. Chen, and Y. Y. Du, "Large recovery strain in Fe-Mn-Si-based shape memory steels obtained by engineering annealing twin boundaries," *Nature Communications*, vol. 5, article 4964, 2014.

[17] M. Koster, W.J. Lee, M. Schwarzenberger, and C. Leinenbach, "Cyclic deformation and structural fatigue behavior of an FE–Mn–Si shape memory alloy," *Materials Science and Engineering: A*, vol. 637, pp. 29–39, 2015.

[18] H. Peng, J. Chen, Y. Wang, and Y. Wen, "Key factors achieving large recovery strains in polycrystalline Fe–Mn–Si–based shape memory alloys: a review," *Advanced Engineering Materials*, vol. 20, no. 3, article 1700741, 2018.

[19] H. Otsuka, H. Yamada, T. Maruyama, H. Tanahashi, S. Matsuda, and M. Murakami, "Effects of alloying additions on Fe-Mn-Si shape memory alloys," *ISIJ International*, vol. 30, no. 8, pp. 674–679, 1990.

[20] S. Kajiwara, D. Liu, T. Kikuchi, and N. Shinya, "Remarkable improvement of shape memory effect in Fe-Mn-Si based shape memory alloys by producing NbC precipitates," *Scripta Materialia*, vol. 44, no. 12, pp. 2809–2814, 2001.

[21] S. Farjami and H. Kubo, "Elastic energy analysis of carbide and nitride-type precipitates in an Fe–Mn–Si–Cr shape memory alloy," *Materials Transactions*, vol. 47, no. 3, pp. 571–579, 2006.

[22] A. V. Druker, A. Perotti, I. Esquivel, and J. Malarría, "Design of devices and manufacturing of Fe-Mn-Si shape memory alloy couplings," *Procedia Materials Science*, vol. 8, pp. 878–885, 2015.

[23] A. Cladera, B. Weber, C. Leinenbach, C. Czaderski, and M. Motavalli, "Iron-based shape meory alloys for civil engineering structures: an overview," *Construction and Building Materials*, vol. 63, pp. 281–293, 2014.

[24] N. Cimpoeşu, L. C. Trincă, G. Dascălu, S. Stanciu, S. O. Gurlui, and D. Mareci, "Electrochemical characterization of a new biodegradable FeMnSi alloy coated with hydroxyapatite-zirconia by PLD technique," *Journal of Chemistry*, vol. 2016, Article ID 9520972, 9 pages, 2016.

[25] T. Saito, K. Gąska, A. Takasaki, and C. Kapusta, "Fe–Mn–Si alloy by mechanical alloying and direct current sintering," *Journal of Mechanical Engineering*, vol. 30, pp. 62–67, 2010.

[26] C. Suryanarayana, "Mechanical alloying and milling," *Progress in Materials Science*, vol. 46, no. 1-2, pp. 1–184, 2001.

[27] T. Saito, C. Kapusta, and A. Takasaki, "Synthesis and characterization of Fe–Mn–Si shape memory alloy by mechanical alloying and subsequent sintering," *Materials Science and Engineering: A*, vol. 592, pp. 88–94, 2014.

[28] Y. H. Wen, M. Yan, and N. Li, "Effects of carbon addition and aging on the shape memory effect of Fe–Mn–Si–Cr–Ni alloys," *Scripta Materialia*, vol. 50, no. 4, pp. 441–444, 2004.

[29] X. H. Min, T. Sawaguchi, K. Ogawa, T. Maruyama, F. X. Yin, and K. Tsuzaki, "An attempt to lower Mn content of Fe–17Mn–6Si–0.3C shape memory alloy," *Journal of Alloys and Compounds*, vol. 577, pp. S478–S482, 2013.